

Geometric properties of graph layouts optimized for greedy navigation

Sang Hoon Lee^{1,2} and Petter Holme^{1,3,4}

¹*IceLab, Department of Physics, Umeå University, 901 87 Umeå, Sweden*

²*Oxford Centre for Industrial and Applied Mathematics, Mathematical Institute, University of Oxford, Oxford OX1 3LB, United Kingdom*

³*Department of Energy Science, Sungkyunkwan University, Suwon 440-746, Korea*

⁴*Department of Sociology, Stockholm University, 106 91 Stockholm, Sweden*

(Dated: August 16, 2021)

The graph layouts used for complex network studies have been mainly been developed to improve visualization. If we interpret the layouts in metric spaces such as Euclidean ones, however, the embedded spatial information can be a valuable cue for various purposes. In this work, we focus on the navigational properties of spatial graphs. We use an recently user-centric navigation protocol to explore spatial layouts of complex networks that are optimal for navigation. These layouts are generated with a simple simulated annealing optimization technique. We compared these layouts to others targeted at better visualization. We discuss the spatial statistical properties of the optimized layouts for better navigability and its implication.

PACS numbers: 89.40.-a, 89.75.Fb, 89.75.-k

I. INTRODUCTION

One of the quintessential properties of spatial structures is to support human navigation, or give cities, buildings etc. their *navigability*. Navigability in purely topological (not spatially embedded) graphs or networks have been studied, especially during the last decade of complex network research [1]. Navigability in more relevant context of spatial networks [2], however, is a more recent topic [3]. As a contribution to this topic, we have introduced greedy spatial navigation (GSN) as a simple probe of the effects of human cognitive limitation to navigation in non-familiar environments [4, 5]. The essence of GSN is the quantification of navigability for *given* spatial structures. In this work, we focus on the reverse problem of *giving* spatial structures for better navigability.

In our previous work, we made the observation that a spring-embedding layout (for better visualization) actually helps the greedy navigators to find better routes compared to a random layout [4]. The difference is occasionally very large, depending on the network structure. This “side effect” comes from the property that layouts for visualization usually put topologically close vertex pairs geometrically close. In this paper, we study the layouts optimized solely for the better greedy navigability. In particular, we focus on geometric characteristics of optimized layouts compared to the aforementioned visualization oriented layouts. The optimization is done by simulated annealing (SA) process [6]. This will be further discussed in the next section.

II. LAYOUT OPTIMIZATION PROCEDURE

We begin the optimization procedure by assigning a random position for each vertex independently, inside square of unit length. The object function to minimize is the average steps greedy navigators take for all the vertex pairs as source–target (s – t) ones (denoted as d_g in Ref. [5]). We use the SA [6] technique that repeatedly applies the heating and quenching processes. At each time step, the position of a randomly

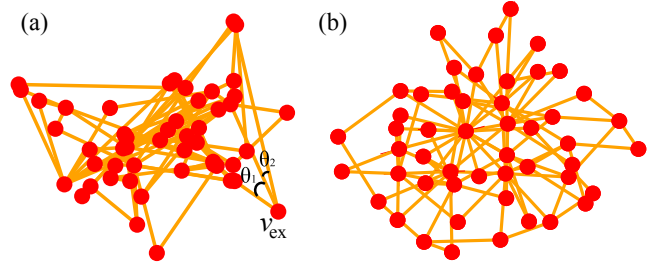


FIG. 1: (color online) Examples of the optimal (a) and KK layout (b) of the BA model. The GSN pathway is 3.85 (4.79) for the optimal (KK) layout, respectively.

chosen vertex, whose coordinates are (x_0, y_0) , is relocated to $(x_0 + \Delta x, y_0 + \Delta y)$ where Δx and Δy are randomly drawn from the interval $[-l, l]$ ($l \gg 1$) uniformly. In the heating (quenching) process, such a trial movement is accepted if d_g is decreased, while it is accepted with the probability p_{high} (p_{low}) otherwise, respectively. This is similar to successful heuristic methods in combinatorial optimization [7]. The trial movement in the heating process is repeated for T_H times in the unit of Monte Carlo (MC) steps, where one step is defined as N (the number of vertices) trial movement. On the other hand, in the quenching process, the trial movement is repeated until consecutive T_L times (again, in the unit of MC steps) of rejection occurs. Overall, these consecutive heating and quenching processes as a single session are repeated T_{HL} times in total. Finally, during this procedure, the layout L_{min} corresponding to the minimum d_g value up to present is recorded and constantly updated if a new minimum d_g occurs. With the method, after the SA procedure ends, we obtain the approximated optimal layout for GSN up to the moment.

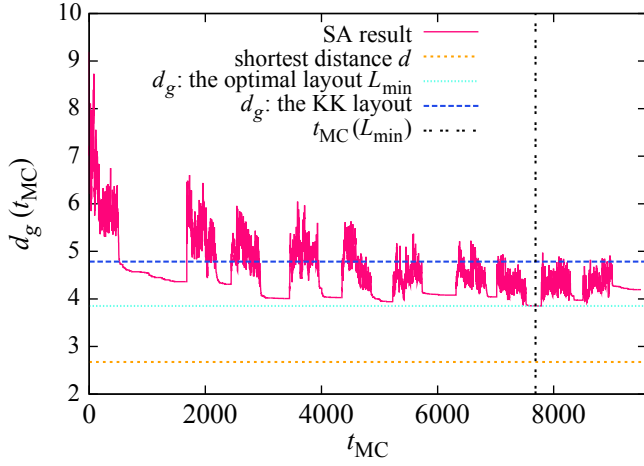


FIG. 2: (color online) A typical time series of d_g in the unit of MC steps t_{MC} , in case of the BA model used in Fig. 1, along with the real shortest path length d , d_g for the optimal layout L_{min} [Fig. 1(a)] and the KK layout [Fig. 1(b)], and the moment of L_{min} denoted as the vertical line.

III. RESULTS

To start our exploration, we set $l = 10$, $p_{high} = 0.2$, $p_{low} = 0$ (completely frozen phase), $T_H = 500$, $T_L = 100$, and $T_{HL} = 10$. Due to the computational complexity we present the results using the graphs with rather small sizes: $N = 50$, in case of Barabási–Albert (BA) [8], Holme–Kim (HK) [9], Watts–Strogatz (WS) [10] model graphs, where the average degree is set as $\bar{k} = 2$ for BA and HK and $\bar{k} = 4$ for WS graphs (triangle formation probability for HK model is 1 and the rewiring probability for WS model is 0.1). As an example of real-world graph, we analyze the social network of the oft-studied Zachary karate club with $N = 34$ [11]. As representative examples of completely regular structures, the two-dimensional square lattice (2D square) with the open boundary condition with $N = 7 \times 7 = 49$ and the one-dimensional ring (1D ring) with $N = 50$ and $k = 2$ (connected only with the nearest neighbors) are analyzed as well. A typical example of L_{min} and time series of d_g in case of the BA model is illustrated in Figs. 1(a) and 2.

In our further analysis we first investigate the angle (defined as the undivided angles between edge pairs attached to each vertex—in Fig. 1 this means we include θ_1 and θ_2 but not $\theta_1 + \theta_2$) distributions of optimal layouts for GSN, in comparison to the spring-embedding Kamada–Kawai (KK) layout for the purpose of visualization [12], as shown in Fig. 3. An example of L_{min} and time series of d_g in case of the KK layout is shown in Figs. 1(b) and 2. Even if it is demonstrated that the KK layout is helpful for GSN compared to the random navigation [4], the optimal layout shows significantly different angular profiles to the ones in KK layout. In particular, much sharper angles dominate the former case, in contrast to the latter case composed of a certain range of characteristic angles for better visualization. Among the optimized layouts, the graphs with hubs (vertices with large numbers of neigh-

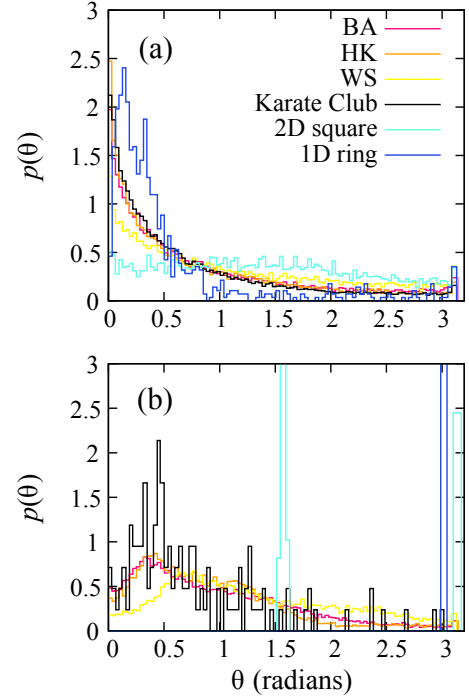


FIG. 3: (color online) Distribution of angles in the optimized (a) and KK (b) layout. At least 39 graph ensembles are used to average for all the cases.

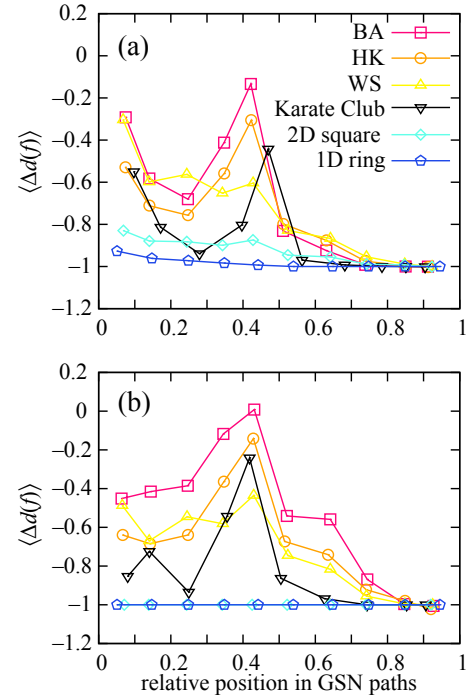


FIG. 4: (color online) Average step decreased along the GSN paths in terms of the relative position f along the pathways, in the optimized (a) and KK (b) layout. At least 39 graph ensembles are used to average for all the cases, and the horizontal axis is equipartitioned into 10 bins.

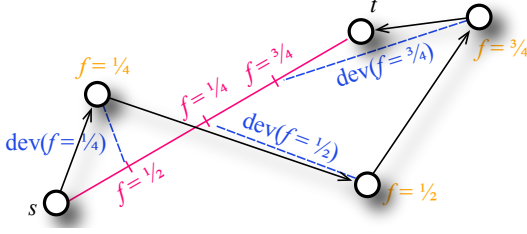


FIG. 5: (color online) An illustration of the definition of deviation from the straight line for a s - t pair. Each intermediate vertex's location in the GSN pathway of length 4 (arrows) is compared to the corresponding intermediate points (green dots) equally spaced in the straight line (red line). The deviation for each intermediate point is defined as the Euclidean distance between the two points (blue dashed lines), in the unit of the straight line.

bors) such as the BA, HK, and Karate Club graphs, are obviously dominated by more sharper angles attached to the hubs than the WS graph case.

For a deeper investigation of GSN pathways, we analyze the average distance (number of edges in the shortest path to the target) decreased along the GSN pathway. We denote this quantity as $\langle \Delta d(f) \rangle$ and present in Fig. 4, where the relative position in a pathway is denoted as the fraction $f = n/d_g$ ($n = 1, \dots, d_g - 1$) for the n 'th intermediate vertex. As seen, for all the graphs, $|\langle \Delta d(f) \rangle|$ is larger for the KK layout than for the optimal layout in the early stage of the GSN pathways. However, the optimal pathway shows larger $|\langle \Delta d(f) \rangle|$ soon afterwards, which leads to better performance (shorter GSN pathways). Another aspect is the peak of $\langle \Delta d(f) \rangle$ for both the KK and optimal layouts, indicating the characteristic intermediate peak (point of inefficiency) in the GSN pathways.

In contrast to the random graph models (BA, HK, and WS) and Karate Club graph, in case of the regular lattices (2D square and 1D ring) the KK layout provides the exactly optimal layout for GSN, where the topological square lattice is mapped to a geometrical square lattice with almost right angles. This can be seen from the peaks of Fig. 3(b). The topological 1D ring network is laid out as a circle (with almost straight angles as shown in the peak in Fig. 3(b)), and by $\langle \Delta d(f) \rangle = -1$ regardless of f in Fig. 4(b)). The SA algorithm, however, shows a suboptimal performance for such regular structures as shown in Figs. 3(a) and 4(a), in contrast to the KK layout very good at detecting such regular structures.

Another way to explore the GSN pathways is to measure their straightness, by comparing the pathways to the straight line connecting s - t pairs. Similar to the analysis of $\langle \Delta d(f) \rangle$, we quantify the local straightness as a function of f , as illustrated in Fig. 5. The deviation from the straight line connecting a s - t pair, represented as a vector \mathbf{v}_{st} from s to t , at f is denoted as $\text{dev}(f)$ —the Euclidean distance between the intermediate vertex at f and the point at the same fraction f on the straight line. Note that all the distance measures for each s - t pair are scaled with respect to the length of the straight line ($|\mathbf{v}_{st}| = 1$), to facilitate the comparison between all the different paths and layouts. Furthermore, each vector $\text{dev}(f)$ (whose direction is from the point on the straight line to the

vertex on the GSN pathway) for the distance $\text{dev}(f)$ is decomposed into the component parallel to the straight line $\text{dev}_{\parallel}(f)$ and the one perpendicular to it $\text{dev}_{\perp}(f)$. Due to the intrinsic directionality from the source to the target, $\text{dev}_{\parallel}(f)$ can be positive or negative depending on the angle between \mathbf{v}_{st} and $\text{dev}(f)$, and we take the positive value of $\text{dev}_{\perp}(f)$ for convenience.

For the optimized and KK layouts applied to the graphs we have used, values of average deviation from the straight lines as a function of f are presented in Fig. 6— $\langle \text{dev}(f) \rangle$, $\langle \text{dev}_{\parallel}(f) \rangle$, and $\langle \text{dev}_{\perp}(f) \rangle$ separately. From the results, we observe that in most cases the GSN pathways with KK layouts show much less deviation from the straight lines than with the optimized layouts. At a first glance, it may seem counterintuitive, because the GSN routes are shorter in the optimized except for 2D square and 1D ring cases. It is, however, reasonable if one recalls the fact that the path length is defined as the hopping distance (number of edges along a pathway), so that optimized layouts can have much longer edges compared to the KK ones [compare Figs. 1(a) and (b)]. Such longer edges amplify the entire length scale of optimized layouts compared to KK ones. Therefore, in case of hopping-distance-based optimized layouts, the absolute values of deviation themselves are not quite comparable to different types of layouts. However, for a single type of layout, we can compare the effects of different graph topologies. For instance, the (purely topological) BA model shows the largest deviation in most cases, related to the amount of embedded geometric information [4]. The circular trajectories of GSN pathways in the 1D ring case are clearly reflected in the concave curves of $\text{dev}(f)$ and $\text{dev}_{\perp}(f)$ and the slightly negative (positive) $\text{dev}_{\parallel}(f)$ for small (large) f , respectively, for both optimized and KK layouts. It would be interesting if we adopt the alternative definition of path length, for instance, the sum of Euclidean distance along the path [13] and compare the results.

IV. SUMMARY AND DISCUSSIONS

We have investigated the properties of optimized spatial graph layouts for GSN generated by a simple SA process. From the observed geometrical measures, it is shown that, in general, the optimized layouts are characterized by sharp angles and point of inefficiency in the middle of the GSN processes. These properties are qualitatively different from the layouts for better visualization, namely the KK ones, showing the dominating intermediate angles within characteristics ranges. A closer inspection of the navigational routes also reveals that the inefficiency of KK layouts soon follows its initially better performance compared to the optimized ones. In other words, our simulation shows that it is possible to generate GSN-friendly layouts other than the visualization-friendly layouts by just taking the simple SA optimization process.

Our simple SA optimization process, however, also shows its limitation by yielding the suboptimal results for completely regular structures such as the 1D ring and 2D square lattice, where the KK layouts happen to coincide with the exact solution of optimization for GSN. The SA optimization certainly

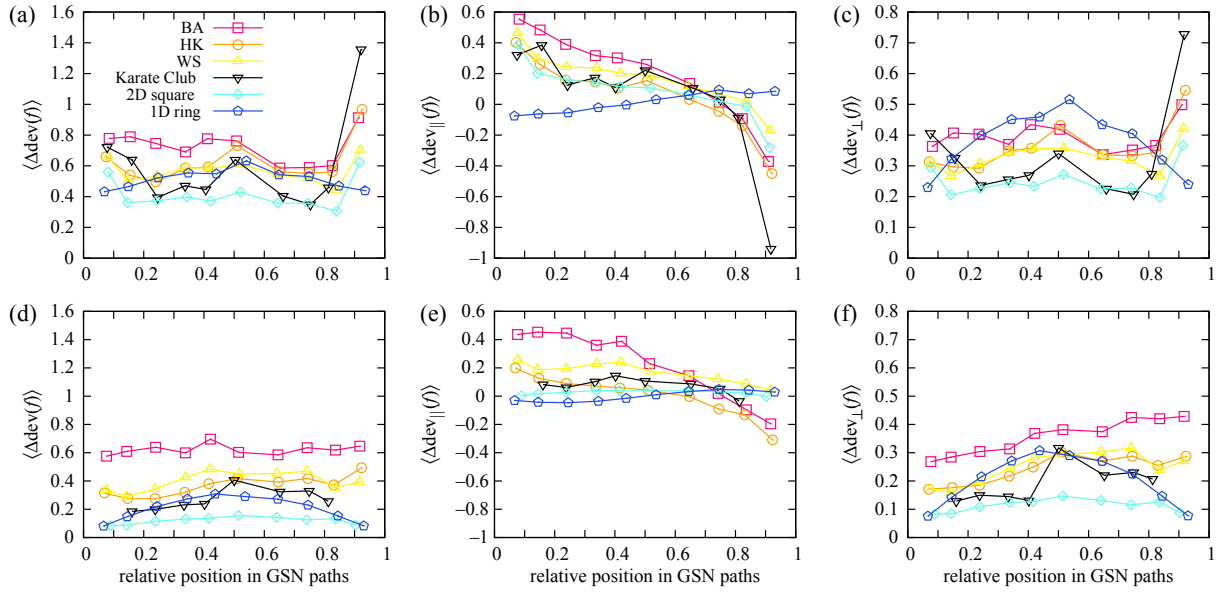


FIG. 6: (color online) Average deviation from the straight line connecting s - t pairs, for the relative position x in the GSN pathways and straight lines. Upper (lower) panels correspond to the optimized (KK) layouts, respectively. $\langle \text{dev}(f) \rangle$ [(a) and (d)] is decomposed into $\langle \text{dev}_{\parallel}(f) \rangle$ [(b) and (e)] and $\langle \text{dev}_{\perp}(f) \rangle$ [(c) and (f)] with respect to the straight line. At least 39 graph ensembles are used to average for all the cases. The horizontal axis is binned into 10 equidistant intervals.

gets close to the exact optimal layout, but not perfectly, at least in our simulation setting. Besides such possible suboptimal performances, the observed properties of optimized layouts for better navigation can, we believe, give valuable hints for constructing various spatial structures in practice, e.g., the urban planning and architecture [14]. Adopting more sophisticated optimization processes and studies on diverse graph structures would be a natural candidate for the future work, for even better understanding of the tripartite relationship of

topology-geometry-navigability.

Acknowledgments

This research is supported by the Swedish Research Council and the WCU program through NRF Korea funded by MEST R31-2008-10029 (PH).

-
- [1] S. N. Dorogovtsev and J. F. F. Mendes, *Adv. Phys.* **51**, 1079 (2002); R. Albert and A.-L. Barabási, *Rev. Mod. Phys.* **74**, 47 (2002); M. E. J. Newman, *SIAM Rev.* **45**, 167 (2003); S. Boccaletti, V. Latora, Y. Moreno, M. Chavez, and D.-U. Hwang, *Phys. Rep.* **424**, 175 (2006).
 - [2] M. Barthélemy, *Phys. Rep.* **499**, 1 (2011).
 - [3] M. Rosvall, A. Trusina, P. Minnhagen, and K. Sneppen, *Phys. Rev. Lett.* **94**, 028701 (2005); H. Youn, M. T. Gastner, and H. Jeong, *Phys. Rev. Lett.* **101**, 128701 (2008); M. Boguñá, D. Krioukov, and K. C. Claffy, *Nature Phys.* **5**, 74 (2008); M. Boguñá and D. Krioukov, *Phys. Rev. Lett.* **102**, 058701 (2009).
 - [4] S. H. Lee and P. Holme, *Physica A* **390**, 3996 (2011).
 - [5] S. H. Lee and P. Holme, *Phys. Rev. Lett.* **108**, 128701 (2012).
 - [6] S. Kirkpatrick, C. D. Gelatt Jr., and M. P. Vecchi, *Science* **220**, 671 (1978).
 - [7] J. Ardelius and E. Aurell, *Phys. Rev. E* **74**, 037702 (2006).
 - [8] A.-L. Barabási and R. Albert, *Science* **286**, 509 (1999).
 - [9] P. Holme and B. J. Kim, *Phys. Rev. E* **65**, 026107 (2002).
 - [10] D. J. Watts and S. H. Strogatz, *Nature* **393**, 409 (1998).
 - [11] W. W. Zachary, *J. Anthropol. Res.* **33**, 452 (1977).
 - [12] T. Kamada and S. Kawai, *Inform. Process. Lett.* **31**, 7 (1989).
 - [13] S. H. Lee and P. Holme, e-print arXiv:1205.0537 (to appear in *Eur. Phys. J.-Spec. Top.*).
 - [14] B. Hillier and J. Hanson, *The Social Logic of Space* (Cambridge University Press, Cambridge, U.K., 1984); L. A. Carlson, C. Hölscher, T. F. Shipley, and R. C. Dalton, *Curr. Dir. Psychol. Sci.* **19**, 284 (2010).